RM E55H29a

NACA

RESEARCH MEMORANDUM

EFFECT OF HIGH ROTOR PRESSURE-SURFACE DIFFUSION ON PERFORMANCE OF A TRANSONIC TURBINE

By James W. Miser, Warner L. Stewart, and Daniel E. Monroe

Lewis Flight Propulsion Laboratory
Cleveland, Ohio

NATIONAL ADVISORY COMMITTEE
FOR AERONAUTICS

WASHINGTON
November 3, 1955
Declassified May 16, 1958

NACA RM E55H29a

NATIONAL ADVISORY COMMITTEE FOR AERONAUTICS

RESEARCH MEMORANDUM

EFFECT OF HIGH ROTOR PRESSURE-SURFACE DIFFUSION ON PERFORMANCE OF A TRANSONIC TURBINE

By James W. Miser, Warner L. Stewart, and Daniel E. Monroe

SUMMARY

A transonic turbine designed for high diffusion on the rotor pressure surface and low diffusion on the suction surface was investigated experimentally. The performance results of the turbine show that the total-pressure-ratio adiabatic efficiency of the turbine was 0.869 at design specific work and design speed. A comparison of the subject turbine with the most efficient transonic turbine in the present series of investigations showed that the subject turbine, with a 36-percent reduction in solidity, had an efficiency almost as high.

The performance results of six transonic-turbine configurations investigated thus far revealed that the specific blade loss can be correlated better by the sum of the suction-surface and pressure-surface diffusion parameters than by the suction-surface diffusion parameter alone. As the sum of the two diffusion parameters increases, the specific blade loss increases almost linearly. However, considering the relatively small amount of data on high rotor-inlet relative Mach number turbines, it cannot be assumed that this type of correlation is completely valid. Nevertheless, the investigations to date do point out that pressure-surface diffusion, as well as suction-surface diffusion, is an important design consideration.

INTRODUCTION

High rotor-inlet relative Mach number turbines, hereinafter called high Mach number turbines, are particularly important in aircraft jet-engine design because they have higher specific work, higher weight flow per unit frontal area, and possibly fewer stages than more conservative turbines (ref. 1). However, in order to utilize these advantages to a greater extent, the efficiencies of high Mach number turbines must be comparable with those of more conservative design.

Two characteristics of high Mach number turbines which make the job of obtaining high efficiencies rather difficult are low reaction across the rotor and high blade loading. For the case of low reaction, indicated by approximately equal inlet and outlet relative velocities, higher blade loading results in higher diffusion (deceleration) on the rotor-blade surface. In order to obtain low solidities the loading per blade must be high, which results in high diffusion.

The effects of rotor suction-surface diffusion on the performance of four different transonic turbines, which were designed for rotor-hub inlet relative Mach numbers of about 1.0, are discussed in references 2 to 5. For these turbines, it was found that the loss per blade increased markedly with an increase in suction-surface diffusion. Therefore, it is evident that high efficiencies of high Mach number turbines will only be obtained with low diffusion on the suction surface.

With the restrictions of low reaction, high blade loading, and low suction-surface diffusion, a fairly high diffusion must then occur on the pressure surface. Just how high the pressure-surface diffusion should be to minimize the sum of the losses resulting from diffusion and the viscous losses resulting from high solidity (or large wetted area) is not known. Therefore, in order to study the effect of high pressure-surface diffusion on the performance of high Mach number turbines, a transonic-turbine rotor was designed for as high a pressure-surface diffusion as possible without choking the rotor below design weight flow.

The over-all performance of the subject turbine and a comparison of its design-point performance with those of other transonic turbines on the basis of diffusion parameters are presented herein. Also, the results of a survey downstream of the rotor and a discussion of the effect of high pressure-surface diffusion on the location of regions of low local efficiency are given.

TURBINE DESIGN

Design Requirements

The following design requirements for the 14-inch cold-air turbine investigated are nominally the same as those for the reference turbines (see table I):

Equivalent specific work output, $\Delta h'/\theta_{cr}$, Btu/lb	23.03
Equivalent weight flow, $\varepsilon w\sqrt{\theta_{cr}}/\delta$, lb/sec	11.95
Equivalent tip speed, $U_t/\sqrt{\theta_{cr}}$, ft/sec	597

The work output of 23.03 Btu per pound is slightly higher than that for any of the turbines of references 2 to 6, as will be discussed in the section Design Velocity Diagrams.

The symbols used in this report are defined in appendix A. It should be noted that the symbols differ slightly from those used in references 2 to 5, because the symbols were changed to conform with a standard symbol listing in reference 7.

Stator Design

For the subject turbine and the turbine of reference 6, a slightly different stator was used from the one for the turbines of references 2 to 5. The stator was designed for a decrease in trailing-edge thickness from 0.030 inch to 0.010 inch by removal of metal along the suction surface downstream of the throat. As mentioned in reference 6, the decrease in trailing-edge thickness improved the observed design-point efficiency by 0.6 of a point. Therefore, the stator with the thinner trailing edge was used for the subject investigation.

Design Velocity Diagrams

The subject turbine rotor was designed for a slightly different velocity diagram (fig. 1) at stations 5 and 6 from that of the transonic turbines of references 2, 4, 5, and 6 because of a decrease in blockage at the rotor trailing edge. For the reference turbine rotors, a trailing-edge blockage corresponding to 29 blades with 0.050-inch-thick trailing edges was used. In order to have used this same blockage for the subject turbine rotor of 25 blades, the trailing edge would have been unnecessarily thick; therefore, a trailing-edge thickness of 0.030 inch was used.

The reduction in trailing-edge blockage for the same exit whirl as used for the rotors of references 2, 4, 5, and 6 would have reduced the relative velocity just inside the trailing edge. Thus, at the hub the outlet relative velocity would have been lower than the inlet relative velocity, and a slight negative reaction would have occurred. Also, zero diffusion on the suction surface would have been impossible. For these reasons, the exit whirl was increased to provide hub inlet and outlet relative Mach numbers equal to 1.0. This increase in exit whirl changed the design equivalent specific work of the subject turbine to 23.03 Btu per pound as compared with 22.61 Btu per pound for the turbines of references 2, 4, 5, and 6.

The assumptions used in reference 2 were used to obtain the velocity diagrams:

(1) Free vortex flow out of the stator and downstream of the rotor

(2) Simple radial equilibrium throughout the rotor and out of the stator

(3) Total pressure at stator exit equal to 0.97 of stator-inlet total pressure

(4) Over-all adiabatic efficiency of 0.88 based on total pressure to obtain the turbine-outlet total state and velocity diagram at station 6.

Rotor-Blade Design

The rotor-blade design procedure is the same as that used in reference 2 with the following exceptions:

(1) A linear variation in static pressure was assumed to exist along each orthogonal l_o from blade to blade (fig. 2). For the turbines of references 2 and 3, a linear variation in velocity was assumed across the length between the blade surfaces s - t at each axial position. For the turbines of references 4 to 6, a linear variation in static pressure was assumed across the length s - t.

(2) The weight flow crossing the orthogonal surfaces at particular axial stations was determined rather than the weight flow crossing planes perpendicular to the axis of rotation, as in references 2 to 6. The weight flow w was calculated from the equation

$$w = n \int_{r_h}^{r_t} \int_{0}^{l_o} \rho W \, dl_o \, dr \tag{1}$$

(3) For each blade section at each axial station, the angle used in determining the midchannel velocity distribution was the average of the angles β_s and β_p (see fig. 2) between lines parallel to the axis of rotation and the suction and pressure surfaces at either end of the orthogonal. This angle β_{av} was found to be more representative of the average flow angle for the particular weight-flow calculation employed in this case than the mean camber angle φ_c used in the weight-flow calculation of references 2 to 6.

(4) For the weight-flow calculation for each trial configuration of the subject turbine rotor, a zero suction-surface diffusion parameter D_s was originally assumed for the mean section. A mean suction-surface velocity distribution was selected to conform with this D_s. In references 2 to 6 a midchannel velocity distribution was assumed at the hub section.

(5) A curvometer, described in appendix B, was used for measuring curvatures along the surfaces of the blade instead of the radometer described in reference 8 and used in references 2 to 6.

The blade surface velocity distributions for the hub, mean, and tip sections are shown in figure 3. The maximum suction-surface critical velocity ratios at the hub, mean, and tip sections are 1.050, 1.072, and 1.090, respectively. These result in suction-surface diffusion parameters D_S, defined as the difference between the maximum blade surface relative velocity and the blade outlet relative velocity divided by the maximum blade surface relative velocity, equal to 0.048, 0.049, and 0.028 at the hub, mean, and tip, respectively. The minimum critical velocity ratios at the pressure surface are 0.381, 0.384, and 0.339, resulting in pressure-surface diffusion parameters D_p, defined as the difference between the blade inlet relative velocity and the minimum blade surface relative velocity divided by the blade inlet relative velocity, equal to 0.619, 0.487, 0.434 at the hub, mean, and tip sections, respectively.

The rotor consists of 25 blades with solidities at the hub, mean, and tip sections of 2.16, 1.82, and 1.65, respectively.

The rotor-blade coordinates are given in table II, and a sketch of the stator- and rotor-blade passages and profiles is shown in figure 4. A photograph of the 25-blade transonic-turbine rotor assembly is given in figure 5.

APPARATUS, INSTRUMENTATION, AND PROCEDURE

The apparatus, instrumentation, and methods of calculating the performance parameters are the same as those described in reference 2. A diagrammatic sketch of the cold-air turbine test rig is shown in figure 6.

Test runs were made at constant speeds of 60, 80, 90, 100, 110, 120, and 130 percent design speed. For each speed, the total-pressure ratio was varied from approximately 1.4 to the maximum pressure ratio obtainable. Turbine inlet conditions were maintained constant at nominal values of 145° F and 32 inches of mercury absolute.

RESULTS AND DISCUSSION

Performance Results

The over-all performance of the subject transonic turbine is presented by the performance maps in figure 7. In this figure the equivalent specific work $\Delta h'/\theta_{cr}$ is shown as a function of the weight-flow - speed parameter $\varepsilon w\sqrt{\theta}/\delta$ for the various percentages of design speed.

Figure 7(a) presents the over-all performance based on the total-pressure ratio p'_0/p'_6 and the total-pressure-ratio adiabatic efficiency η_t. Figure 7(b) presents the over-all performance based on the rating total-pressure ratio $p'_0/p'_{6,x}$ and the rating total-pressure-ratio adiabatic efficiency η_x. The over-all performance based on the rating total-pressure ratio is included because jet-engine turbines are usually rated in this manner. However, a better evaluation of the turbine aerodynamic performance can be made by basing the results on the total-pressure ratio p'_0/p'_6.

From figure 7(a) it can be seen that the efficiency at design work and design speed is 0.869, and the maximum efficiency is also 0.869. A comparison of design-point efficiencies in figures 7(a) and (b) indicates that the efficiency based on the total-pressure ratio p'_0/p'_6 is 1.9 percentage points higher than that based on the rating total-pressure ratio $p'_0/p'_{6,x}$. This occurs as a result of the slight negative exit whirl designed into the rotor (see. fig. 1).

At design point, the subject turbine is almost as efficient as the most efficient turbine (ref. 6) in the present program of transonic-turbine investigation. The latter has an efficiency at design work and speed of 0.872 and a maximum efficiency of 0.878, as shown in figure 8 by the performance map of the turbine of reference 6. These two transonic turbines have rotors designed for nearly zero suction-surface diffusion parameters; therefore, they provide a good means of studying the change in specific blade loss with an increase in pressure-surface diffusion parameter.

The subject turbine rotor has a 62-percent-higher pressure-surface diffusion parameter D_p than that of reference 6 (see fig. 9 and table I). This large increase in D_p resulted in a large increase in the loss per blade, but a reduction in solidity of 36 percent just about offset the increased loss per blade. This approximate balance of losses indicates that there is a possibility of reducing turbine weight by decreasing the solidity and increasing the pressure-surface diffusion without any penalty in efficiency. However, for the present series of transonic turbines investigated, the rotor-blade hub solidity of 2.16 for the subject turbine is the minimum that can be used without choking the rotor at less than design weight flow regardless of the diffusion possible on the suction and pressure surfaces. The weight-flow restriction results from the large velocity gradients near the blade throat, which are caused by the large spacing between the blades.

Specific Blade Loss

A plot of specific blade loss L against the suction-surface diffusion parameter D_s is shown in figure 10. This figure includes a curve presented in reference 5 for the turbines of references 2 to 5 and the two points for the subject turbine and the turbine of reference 6. The location of the point for the subject turbine obviously makes it necessary to plot L on a different basis in order to obtain correlation. In view of the fact that pressure-surface diffusion is also a contributor to the rotor-blade loss, a plot of L against the sum of the pressure- and suction-surface diffusion parameters $D_p + D_s$ is given in figure 11. This figure gives a better correlation of the specific blade loss for all six turbine configurations and indicates that the specific blade loss may increase as the sum of the two surface diffusion parameters increases. Whether or not D_s and D_p should be added on a par with each other is debatable. Nevertheless, figure 11 shows that adding D_s and D_p directly gives good correlation. Although it is believed that the suction-surface diffusion is of greater importance because of the higher velocity level and the boundary-layer build-up prior to the point where diffusion begins, pressure-surface diffusion is also sufficiently important that it should be considered in the rotor design.

It should be noted that the values of specific blade loss for the subject turbine and the turbine of reference 6 fall below the curve drawn in figure 11. The reason for the lower specific blade loss for these turbines is that the efficiency with the stator used was slightly higher than that with the stator used for the turbines of references 2 to 5 (see Stator Design). The specific blade loss for the turbine of reference 4 is 0.0469 and for the turbine of reference 6 is 0.0449, which represents a decrease in specific blade loss of 0.0020. It is assumed that approximately the same reduction in specific blade loss for the subject turbine resulted from using the modified stator. The data points (fig. 11) for the turbines of references 4 and 6 and for the subject turbine indicate that for each stator there is a curve that could be drawn similar to the one shown.

Survey Results

Detailed radial and circumferential surveys of total temperature and total pressure were made downstream of the turbine rotor with the turbine set at design speed and design work. The results of these surveys are shown in figure 12 as contours of local adiabatic efficiency η_l. The efficiencies below 0.825 occupy a solid band across the blade passage just above the mean section, and the radial width of the band is approximately 20 percent of the blade height. This loss region is significant, because the surveys behind other transonic-turbine rotors show a gradual decrease in local adiabatic efficiency from hub to mean and a

more rapid decrease in efficiency near the tip (see ref. 5). This high loss region can be seen better in figure 13, which shows the radial variation of maximum and minimum local adiabatic efficiency.

Blade-Element Loss Characteristics

In order to study further the loss characteristics of the subject turbine, the rotor-blade-element loss parameter $\bar{\omega}_6 \cos \beta_6/\sigma$ was calculated from the survey results, as in reference 9. The relative total-pressure loss coefficient $\bar{\omega}_6$ based on the measured outlet dynamic pressure is defined by

$$\bar{\omega}_6 = \frac{p_3'' - p_6''}{p_6'' - p_6} \tag{2}$$

Figure 14 is a copy of figure 7 in reference 9 (with the symbols of this report), which gives the blade-element loss parameter at the hub, mean, and tip sections as a function of the suction-surface diffusion parameter D_s for the turbines of references 2 to 5. Also in this figure are the values of the loss parameter for each blade section of the subject turbine. The points for the hub and tip of the subject turbine are close to the curves for the reference turbines, but the point for the mean is considerably above the curve. The locations of the points for the subject turbine with respect to the curves probably result from the difference in the paths taken by the low-momentum fluids resulting from pressure-surface diffusion and those resulting from suction-surface diffusion.

In order to understand the difference between the effects of suction-surface and pressure-surface diffusion, it is necessary to consider the forces acting on the boundary layer in the regions where the diffusions occur. Suction-surface diffusion usually occurs along the last half of the blade where the whirl velocity is less than the blade speed; therefore, the centrifugal force exceeds the static-pressure force, and the low-momentum fluids in the suction-surface boundary layer would move toward the tip. Pressure-surface diffusion usually occurs along the first half of the blade where the whirl velocity is greater than the wheel speed. Therefore, the static-pressure force exceeds the centrifugal force, and the low-momentum fluids in the pressure-surface boundary layer would move toward the hub during their travel over the first half of the blade. But, when the pressure force on the boundary layer reverses itself over the last half of the blade, the low-momentum fluids move back toward the tip. It is also possible that some of the low-momentum fluids moving toward the

hub along the first half of the blade reach the hub boundary layer, cross over to the suction surface as part of the hub boundary layer because of the cross-channel pressure gradient, and then move along, or separate from, the suction surface (see ref. 10). Certainly these boundary-layer flows occur, but the extent to which they could affect turbine performance is different for each turbine, depending on the amount of pressure-surface diffusion and the region in which the diffusion occurs.

For the subject turbine, it is believed that a large amount of the low-momentum fluids resulting from high pressure-surface diffusion moves from the pressure surface to the suction surface as previously outlined, then is centrifuged outward to be measured as a loss near the mean section, as shown in figure 12. This high-loss region near the mean section is also evident from the value of the loss parameter for the mean section, which is considerably above the curve for the reference turbines shown in figure 14. Because pressure-surface and suction-surface diffusions result in different types of radial shifts of low-momentum fluids, it is evident that, in general, correlation of the blade-element loss parameter with the design diffusion of a section is not feasible for three-dimensional blades of the type used in the transonic turbines investigated.

SUMMARY OF RESULTS

A transonic turbine which was designed for approximately zero diffusion on the suction surface and high diffusion on the pressure surface has been investigated experimentally. The significant results are as follows:

1. At design equivalent specific work and speed, the total-pressure-ratio adiabatic efficiency was approximately 0.869.

2. Comparison of the subject turbine with another transonic turbine having almost the same velocity diagrams and suction-surface diffusion parameter showed that the subject turbine lost only 0.3 of a percentage point in efficiency with an increase in the pressure-surface diffusion parameter of 62 percent.

CONCLUSION

The experimental results of five transonic turbines investigated thus far showed that specific blade loss increases almost linearly with the sum of the suction-surface and pressure-surface diffusion parameters.

However, on the basis of the relatively small amount of data on high-velocity turbines, this correlation cannot be assumed completely valid. Nevertheless, the results to date point out that the pressure-surface diffusion, as well as the suction-surface diffusion, is an important design consideration.

Lewis Flight Propulsion Laboratory
National Advisory Committee for Aeronautics
Cleveland, Ohio, August 30, 1955

APPENDIX A

SYMBOLS

The following symbols are used in this report:

D_p pressure-surface diffusion parameter,

$$\frac{\text{blade inlet relative velocity - minimum blade surface relative velocity}}{\text{blade inlet relative velocity}}$$

D_s suction-surface diffusion parameter,

$$\frac{\text{maximum blade surface relative velocity - blade outlet relative velocity}}{\text{maximum blade surface relative velocity}}$$

$\Delta h'$ specific work output, Btu/lb

L specific blade loss, $\frac{1-\eta_t}{\sigma_m}$

l_o orthogonal length, ft

N rotative speed, rpm

n number of blades

p absolute pressure, lb/sq ft

r radius, ft

s blade spacing, ft

t blade thickness in tangential direction, ft

U blade velocity, ft/sec

V absolute gas velocity, ft/sec

W relative gas velocity, ft/sec

w weight flow, lb/sec

β relative gas-flow angle measured from axial direction, deg

γ ratio of specific heats

δ ratio of inlet-air total pressure to NACA standard sea-level pressure, p'_0/p^*

ε $$\frac{\gamma^*}{\gamma}\left[\frac{\left(\frac{\gamma+1}{2}\right)^{\frac{\gamma}{\gamma-1}}}{\left(\frac{\gamma^*+1}{2}\right)^{\frac{\gamma^*}{\gamma^*-1}}}\right]$$

η_l local adiabatic efficiency based on total-state measurements from surveys downstream of rotor

η_t adiabatic efficiency, ratio of turbine work based on torque, weight flow, and speed measurements to ideal work based on inlet total temperature, and inlet and outlet total pressure, both defined as sum of static pressure plus pressure corresponding to gas velocity

η_x rating adiabatic efficiency, same as η_t except outlet total pressure is defined as sum of static pressure plus pressure corresponding to axial component of gas velocity

θ_{cr} squared ratio of critical velocity at turbine inlet to critical velocity at NACA standard sea-level temperature, $(V_{cr,0}/V^*_{cr})^2$

ρ gas density, lb/cu ft

σ solidity, ratio of blade chord to blade pitch

φ angle measured from axis of rotation, deg

$\bar{\omega}_6$ relative pressure loss coefficient based on measured outlet dynamic pressure, $\frac{p''_3 - p''_6}{p''_6 - p_6}$

Subscripts:

av average

c camber

cr conditions at Mach number of 1.0

h hub

m mean

p pressure surface

s suction surface

t tip

u tangential

x axial

0 station upstream of stator (see fig. 1)

1 station at throat of stator passage

2 station at outlet of stator just upstream of trailing edge

3 station at free-stream condition between stator and rotor

4 station at throat of rotor passage

5 station at outlet of rotor just upstream from trailing edge

6 station downstream of turbine

Superscripts:

* NACA standard conditions

' total state

" relative total state

APPENDIX B

PRINCIPLE AND OPERATION OF CURVOMETER

By C. H. Hauser and W. J. Nusbaum

The curvometer shown in figure 15 is an instrument that determines the curvature at a point along an arbitrary curve. Its principle is the same as that of the radometer discussed in appendix C of reference 8, which is based on the fact that three points define a circle.

The principal difference between the radometer and the curvometer is that for the radometer the three points are located by crossed lines and for the curvometer the three points are the points of contact of three circular disks. In both cases, however, two of the points are fixed on a base plate containing a scale and the third point is located on a movable arm pivoted about the fixed center point.

The scale on the radometer is graduated in degrees for measuring the angle between the scale index line on the movable arm and a line through the other two points. The measured angle must then be converted from degrees to curvature, as discussed in reference 3. However, for the curvometer, the scale is graduated directly in curvature; therefore, the intermediate steps of converting degrees to curvature are eliminated.

The curvometer is used in conjunction with a drafting spline which is alined along the curve. The two fixed contact disks are placed against the spline so that the center contact disk is touching the spline at the point where the curvature is to be measured. Then, the movable arm is moved until the third contact disk is touching the spline, and the curvature is read directly on the scale. Because the curvometer uses contact disks, instead of crossed lines as in the case of the radometer, a prediction of the curvature can be made prior to actually drawing the line.

REFERENCES

1. Cavicchi, Richard H., and English, Robert E.: Analysis of Limitations Imposed on One-Spool Turbojet-Engine Designs by Compressors and Turbines at Flight Mach Numbers of 0, 2.0, and 2.8. NACA RM E54F21a, 1954.

2. Stewart, Warner L., Wong, Robert Y., and Evans, David G.: Design and Experimental Investigation of Transonic Turbine with Slight Negative Reaction Across Rotor Hub. NACA RM E53L29a, 1954.

3. Wong, Robert Y., Monroe, Daniel E., and Wintucky, William T.: Investigation of Effect of Increased Diffusion of Rotor-Blade Suction-Surface Velocity on Performance of Transonic Turbine. NACA RM E54F03, 1954.

4. Whitney, Warren J., Monroe, Daniel E., and Wong, Robert Y.: Investigation of Transonic Turbine Designed for Zero Diffusion of Suction-Surface Velocity. NACA RM E54F23, 1954.

5. Whitney, Warren J., Wong, Robert Y., and Monroe, Daniel E.: Investigation of a Transonic Turbine Designed for a Maximum Rotor-Blade Suction-Surface Relative Mach Number of 1.57. NACA RM E54G27, 1954.

6. Whitney, Warren J., Stewart, Warner L., and Wong, Robert Y.: Effect of Reduced Stator-Blade Trailing-Edge Thickness on Over-All Performance of a Transonic Turbine. NACA RM E55H17, 1955.

7. Sectional Committee on Letter Symbols: Letter Symbols for Aeronautical Sciences. ASA Y10.7 pub. by A.S.M.E., 1954.

8. Stewart, Warner L.: Analytical Investigation of Flow Through High-Speed Mixed-Flow Turbine. NACA RM E51H06, 1951.

9. Wong, Robert Y., and Stewart, Warner L.: Correlation of Turbine-Blade-Element Losses Based on Wake Momentum Thickness with Diffusion Parameter for a Series of Subsonic Turbine Blades in Two-Dimensional Cascade and for Four Transonic Turbine Rotors. NACA RM E55B08, 1955.

10. Rohlik, Harold E., Kofskey, Milton G., Allen, Hubert W., and Herzig, Howard Z.: Secondary Flows and Boundary-Layer Accumulations in Turbine Nozzles. NACA Rep. 1168, 1954. (Supersedes NACA TN's 2871, 2909, and 2989.)

TABLE I. - COMPARISON OF DESIGN FEATURES OF SIX TRANSONIC-TURBINE CONFIGURATIONS

Design features		Transonic turbine				
		Ref. 2	Ref. 3	Refs. 4 and 6	Ref. 5	Subject
Equivalent specific work, $\Delta h'/\theta_{cr}$, Btu/lb		22.61	20.20	22.61	22.61	23.03
Equivalent weight flow, $\varepsilon w\sqrt{\theta_{cr}}/\delta$, lb/sec		11.95	11.95	11.95	11.95	11.95
Equivalent tip speed, $U_t/\sqrt{\theta_{cr}}$, ft/sec		597	597	597	597	597
Maximum rotor-blade surface	Mach number	1.28	1.36	1.10	1.57	1.11
	Critical velocity ratio, W/W_{cr}	1.22	1.27	1.08	1.41	1.09
Average design diffusion parameter for -	Suction surface, D_s	0.165	0.306	0.024	0.250	0.042
	Pressure surface, D_p	0.157	0.356	0.316	0.182	0.513
Mean-radius solidity, σ_m		2.81	2.16	2.85	2.36	1.82
Design velocity diagram		Ref. 2	Ref. 3	Ref. 2	Ref. 2	Fig. 1

TABLE II. - ROTOR-BLADE-SECTION COORDINATES

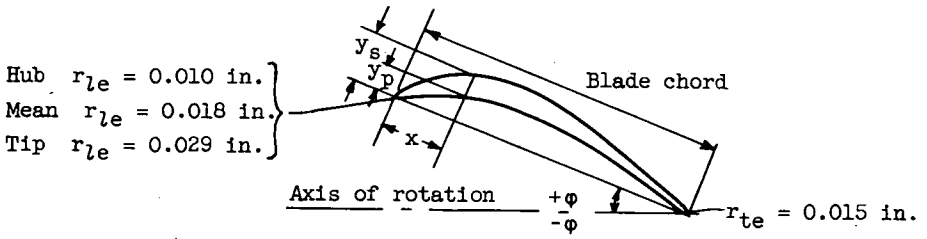

	Hub		Mean		Tip	
			φ, deg			
	-4.5		12.5		23.5	
			r/r_t			
	0.70		0.85		1.00	
x, in.	y_s, in.	y_p, in.	y_s, in.	y_p, in.	y_s, in.	y_p, in.
0	0.010	0.010	0.018	0.018	0.029	0.029
.10	.136	.083	.169	.066	.156	.039
.20	.258	.174	.311	.146	.262	.096
.30	.379	.255	.433	.216	.355	.143
.40	.492	.327	.526	.274	.432	.186
.50	.599	.391	.603	.325	.495	.222
.60	.696	.448	.666	.368	.542	.252
.70	.782	.500	.715	.404	.578	.281
.80	.856	.544	.748	.436	.602	.304
.90	.917	.583	.770	.462	.617	.325
1.00	.962	.617	.777	.482	.622	.343
1.10	.993	.643	.775	.497	.620	.358
1.20	1.008	.666	.763	.508	.611	.369
1.30	1.011	.679	.743	.513	.596	.378
1.40	.997	.685	.713	.514	.574	.382
1.50	.969	.684	.676	.508	.547	.384
1.60	.927	.674	.632	.494	.516	.380
1.70	.870	.654	.583	.475	.481	.372
1.739	-----	-----	-----	-----	.467	-----
1.80	.802	.625	.529	.447	↑	.357
1.844	-----	-----	.505	-----	↑	-----
1.90	.722	.585	↑	.412	↑	.337
2.00	.633	.533	↑	.370	↑	.312
2.098	.544	-----	↑	-----	↑	-----
2.10	↑	.469	↑	.323	↑	.283
2.20	↑	.395	↑	.273	↑	.251
2.30	↑	.312	↑	.220	↑	.217
2.40	↑	.223	↑	.166	↑	.179
2.50	↑	.132	↑	.111	↑	.143
2.60	↑	.038	↑	.055	↑	.107
2.636	.045	.004	↑	-----	↑	-----
2.662	.015	.015	↑	-----	↑	-----
2.693	-----	-----	.037	.002	↑	-----
2.70	-----	-----	.034	.000	↑	.069
2.716	-----	-----	.015	.015	↑	-----
2.80	-----	-----	-----	-----	↑	.031
2.877	-----	-----	-----	-----	.034	.001
2.899	-----	-----	-----	-----	.015	.015

Straight line

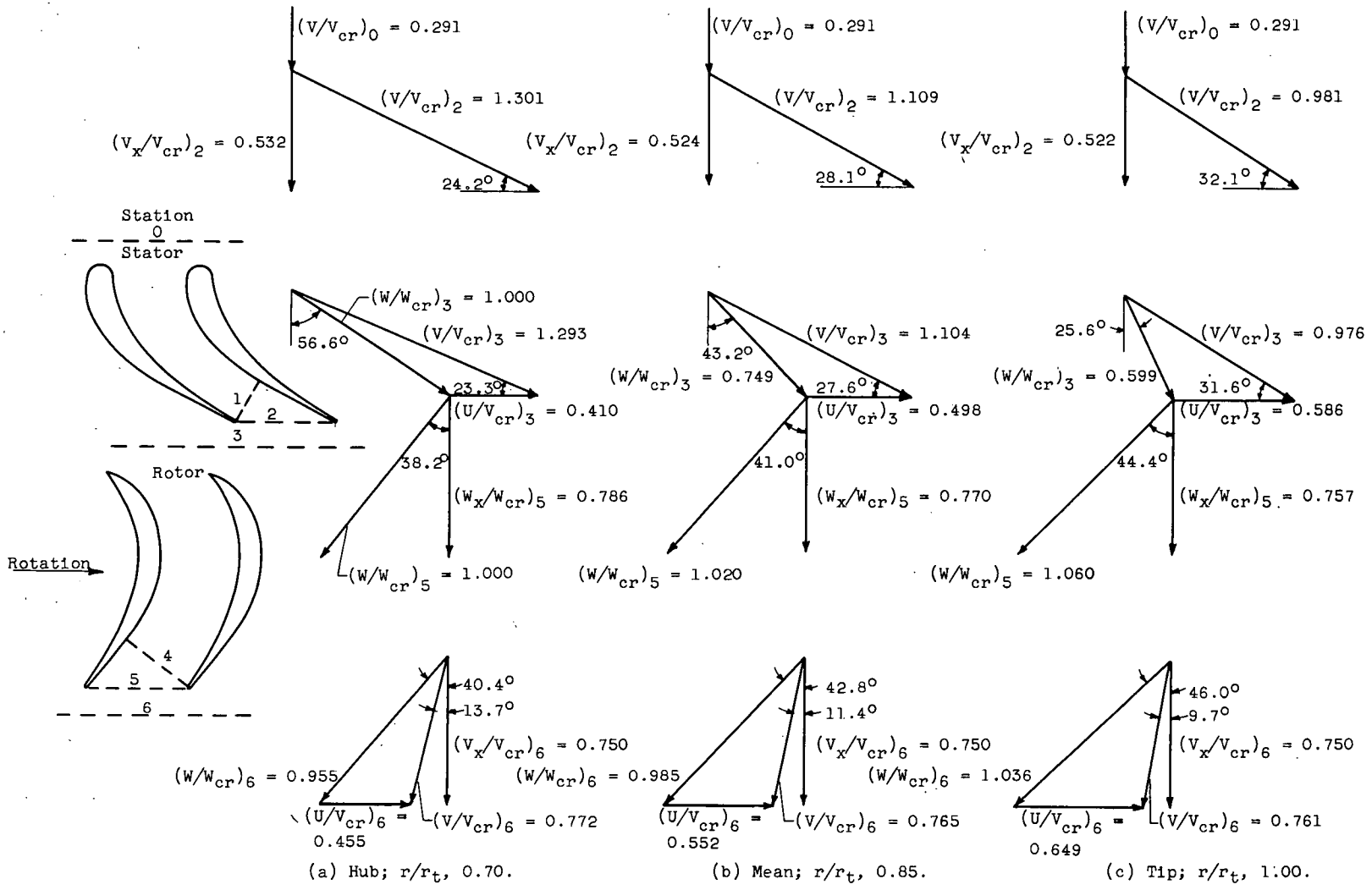

(a) Hub; r/r_t, 0.70. (b) Mean; r/r_t, 0.85. (c) Tip; r/r_t, 1.00.

Figure 1. - Transonic-turbine velocity diagrams.

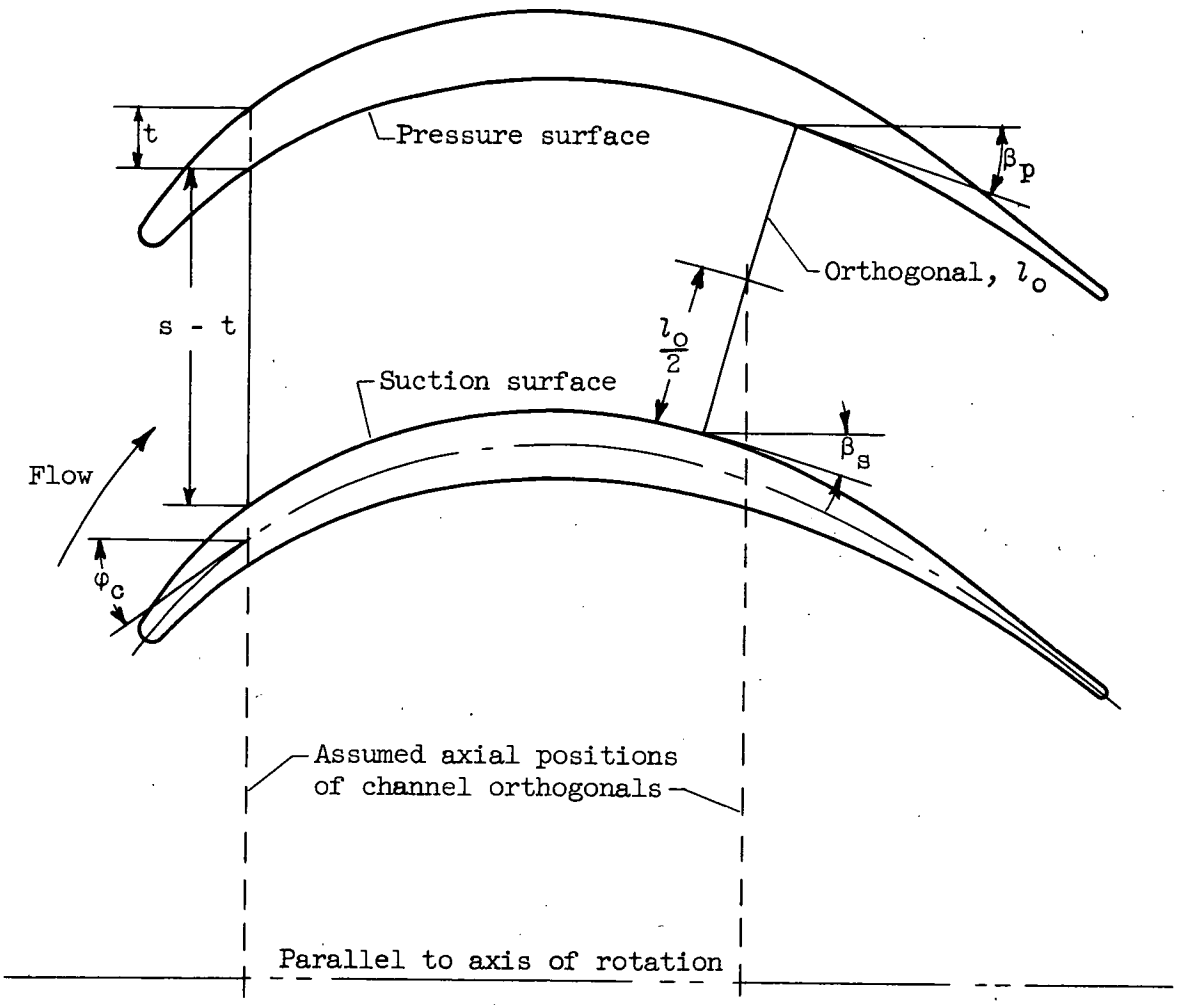

Figure 2. - Some of the important variables in design procedure.

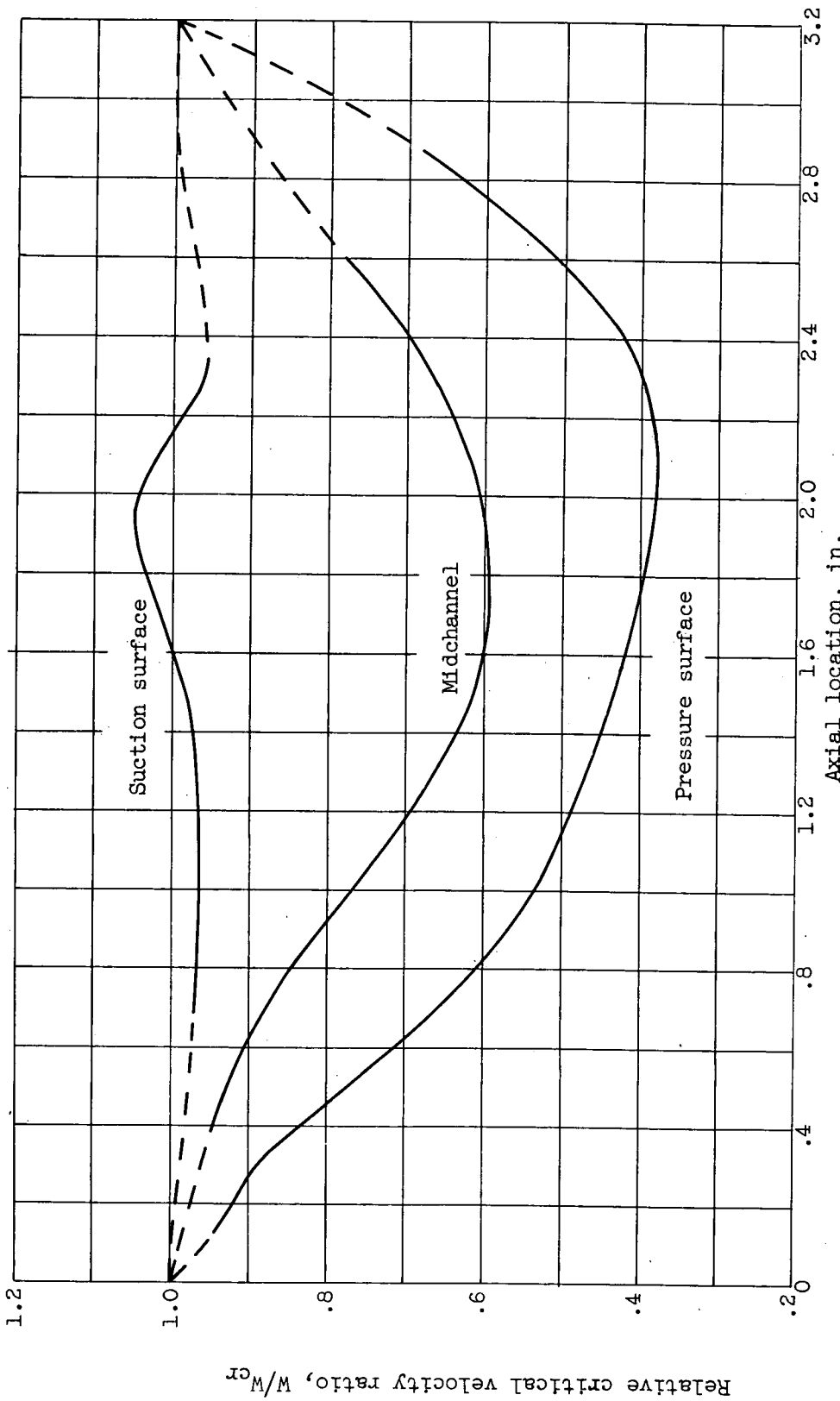

(a) Hub.

Figure 3. - Design rotor midchannel and surface velocity distributions at hub, mean, and tip sections. (Dashed lines denote extrapolation to blade inlet and outlet velocities.)

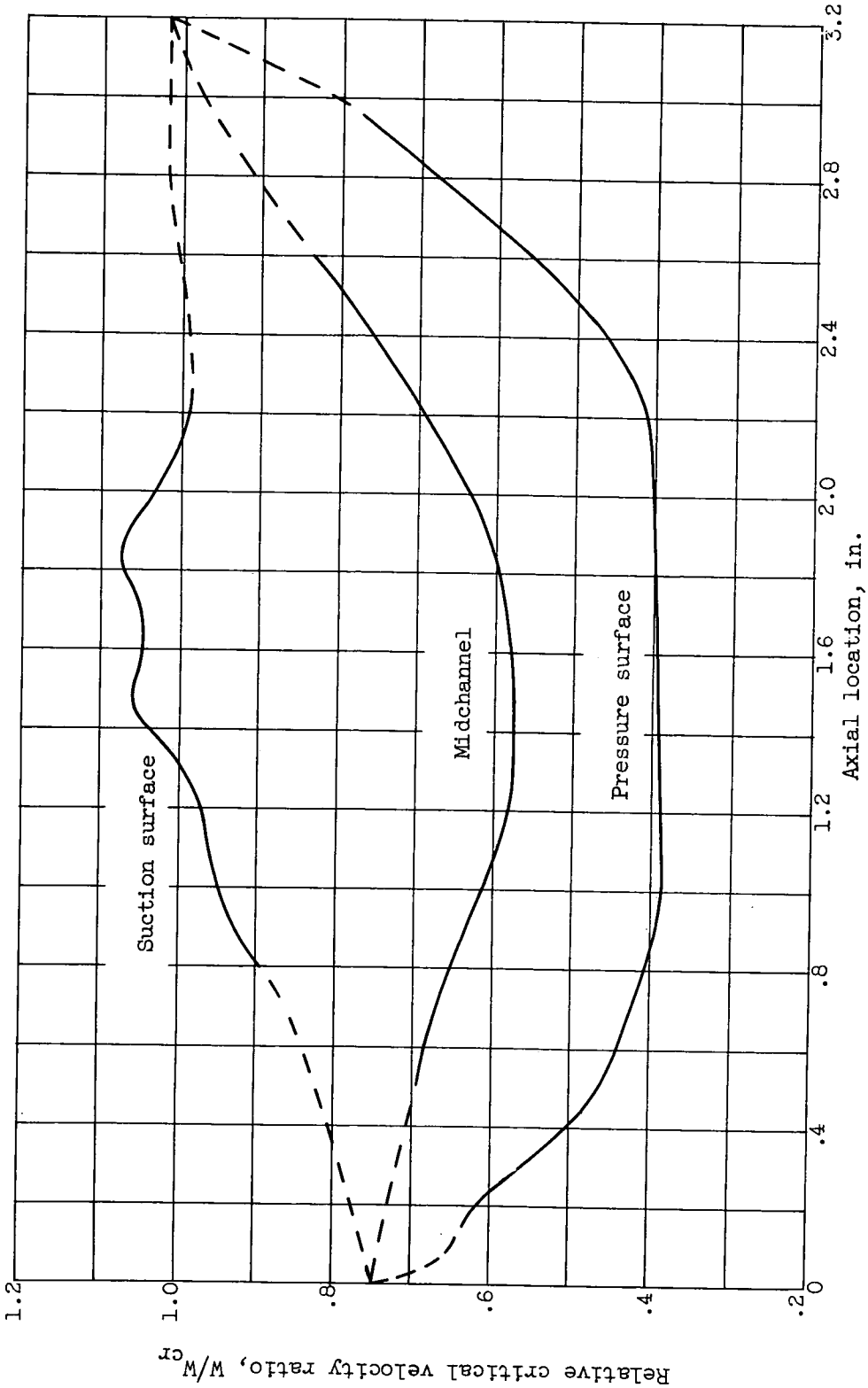

(b) Mean.

Figure 3. - Continued. Design rotor midchannel and surface velocity distributions at hub, mean, and tip sections. (Dashed lines denote extrapolation to blade inlet and outlet velocities.)

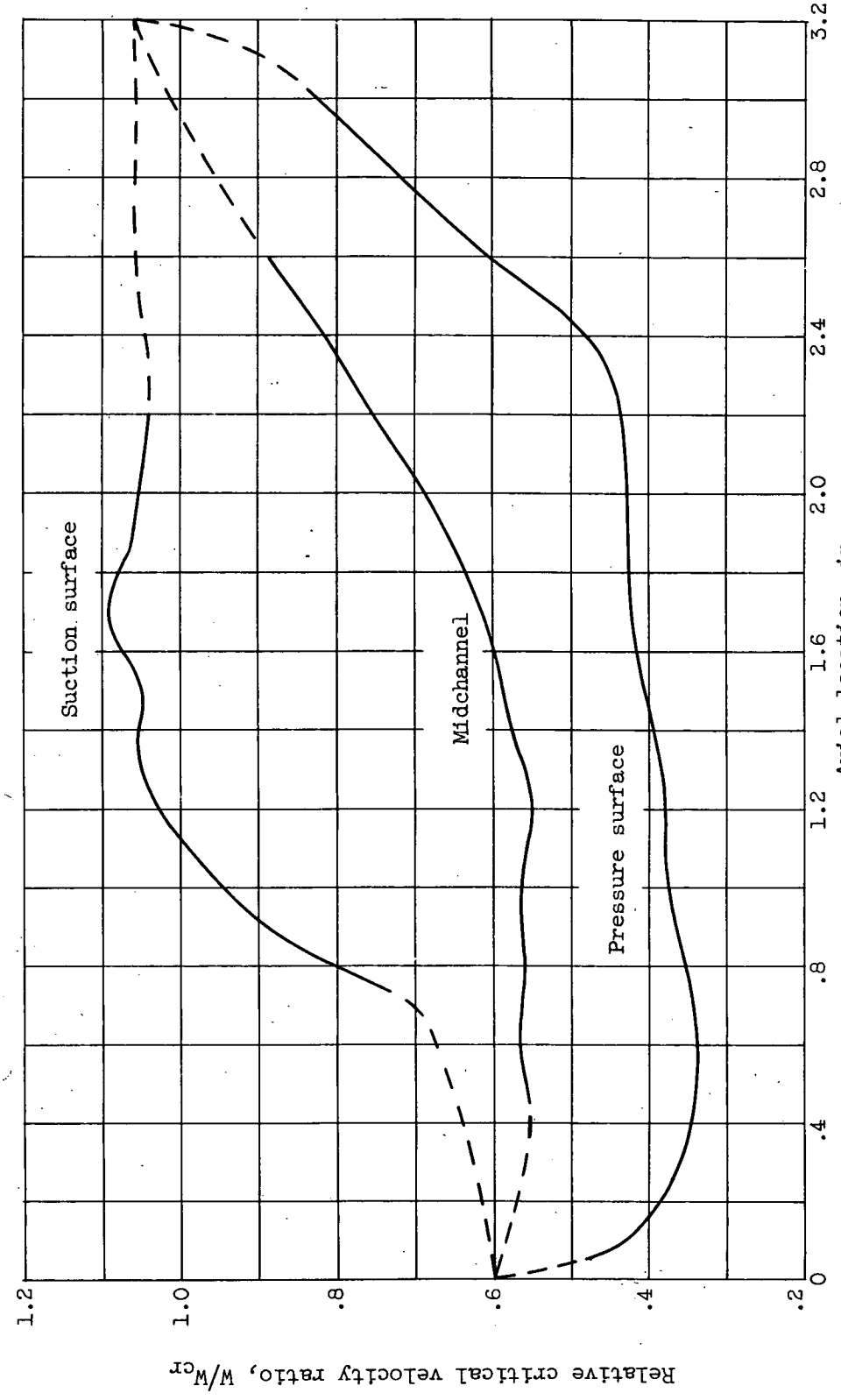

(c) Tip.

Figure 3. - Concluded. Design rotor midchannel and surface velocity distributions at hub, mean, and tip sections. (Dashed lines denote extrapolation to blade inlet and outlet velocities.)

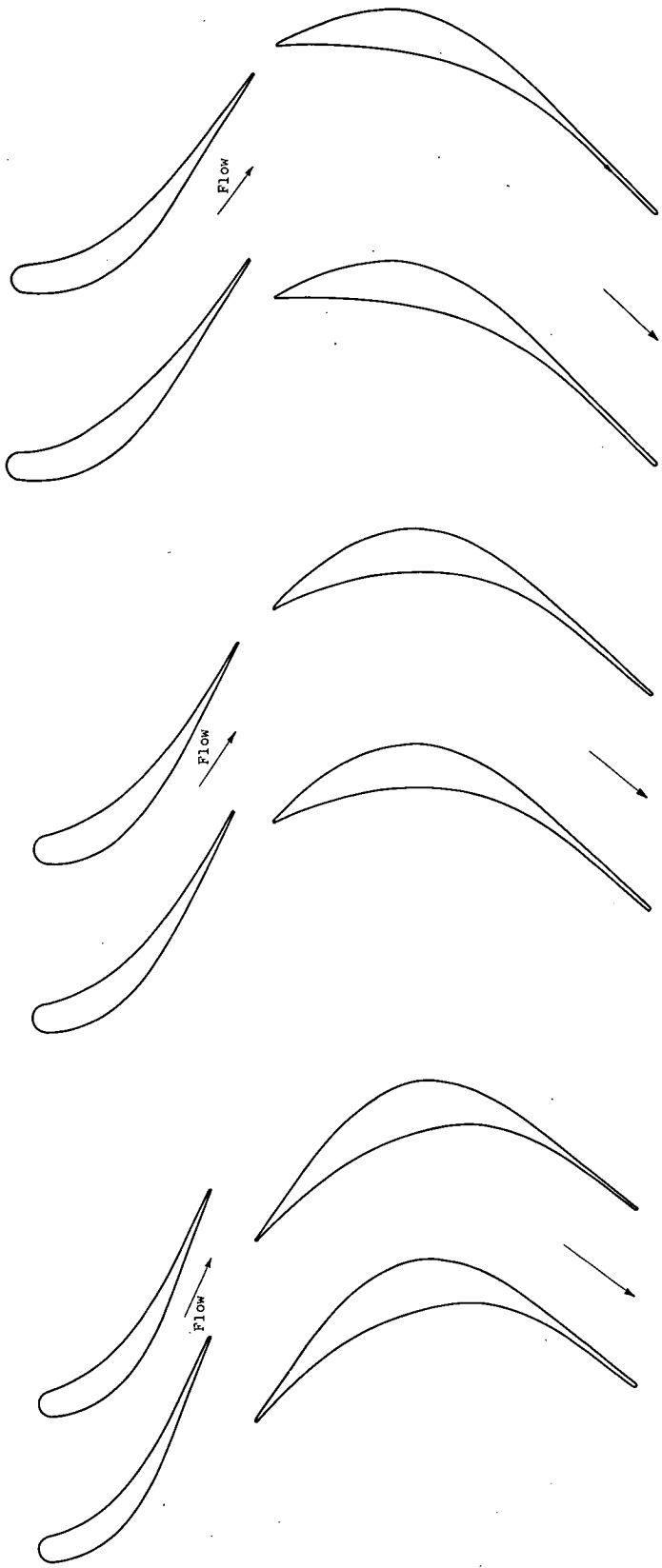

(a) Hub. (b) Mean. (c) Tip.

Figure 4. - Stator- and rotor-blade passages and profiles.

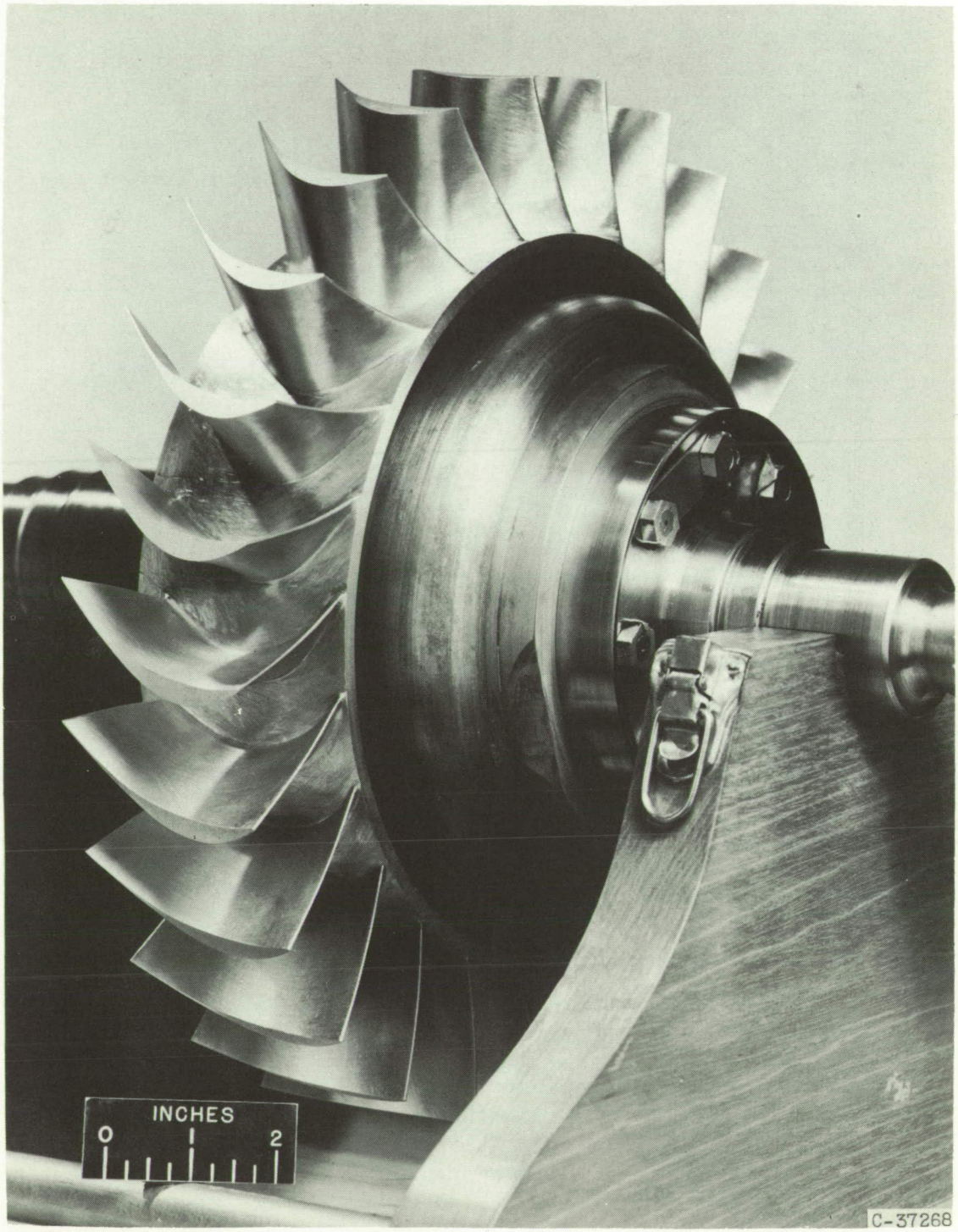

Figure 5. - Photograph of transonic-turbine rotor.

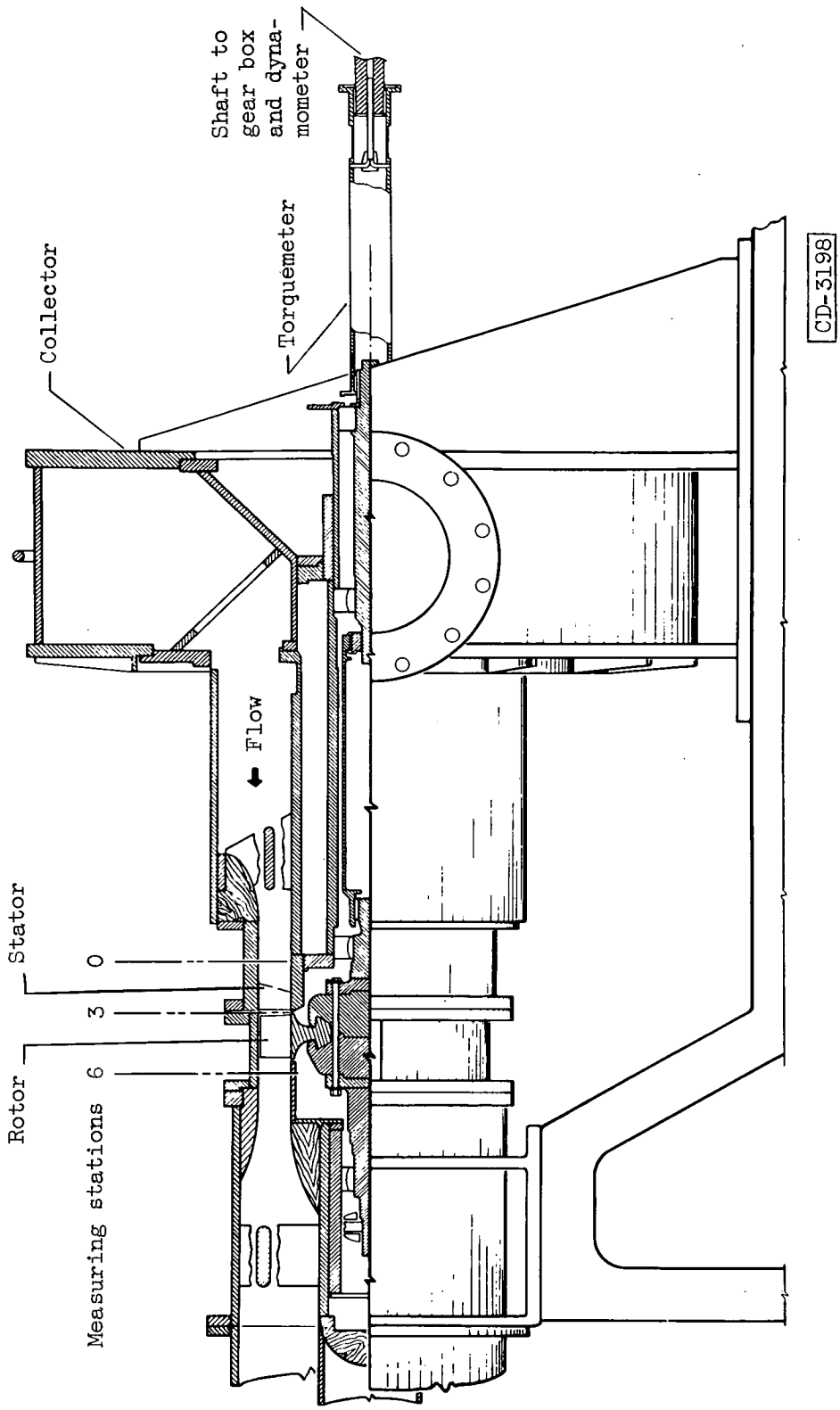

Figure 6. - Diagrammatic sketch of cold-air turbine test section.

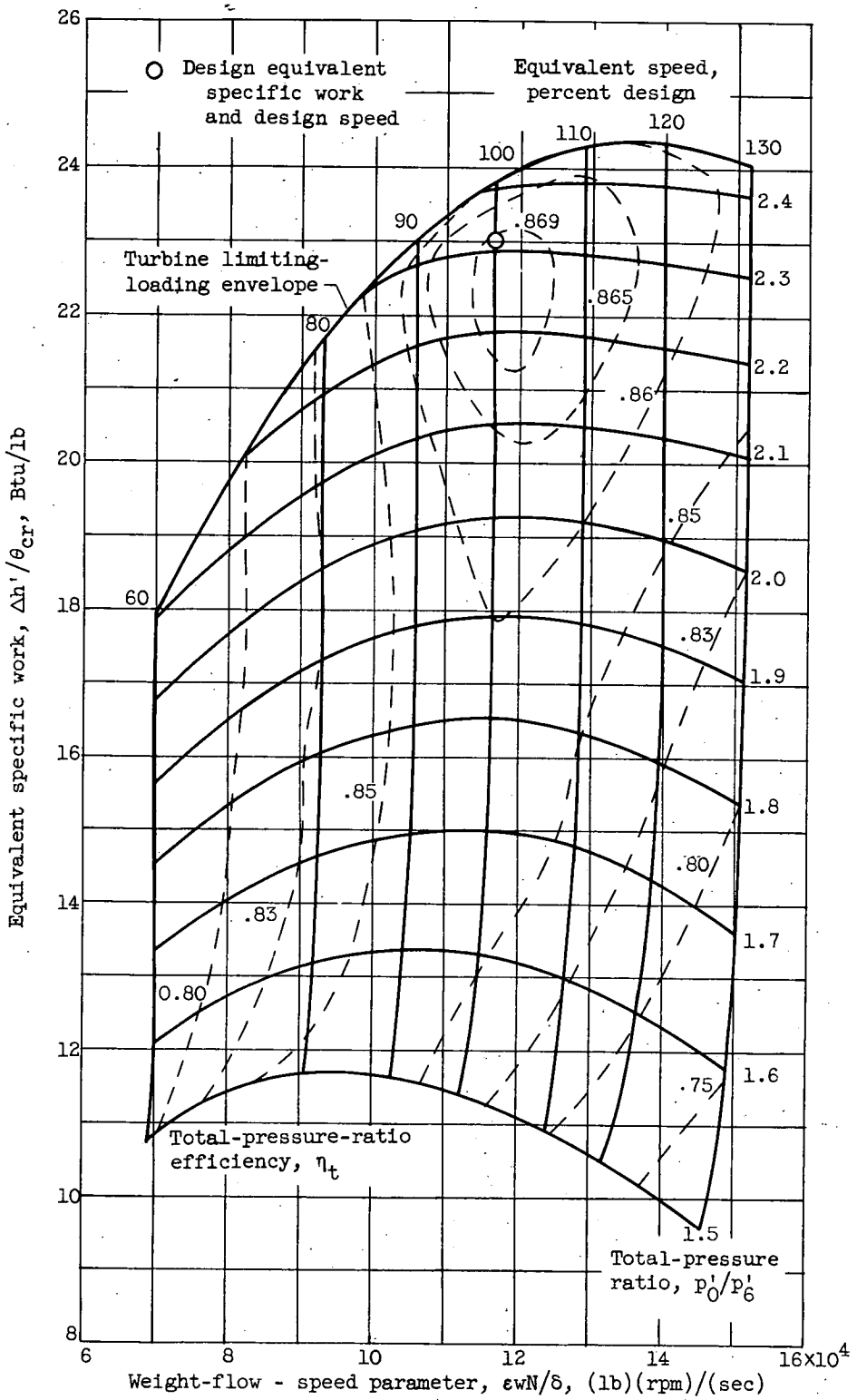

(a) Based on total-pressure ratio across turbine.

Figure 7. - Experimentally obtained performance map.

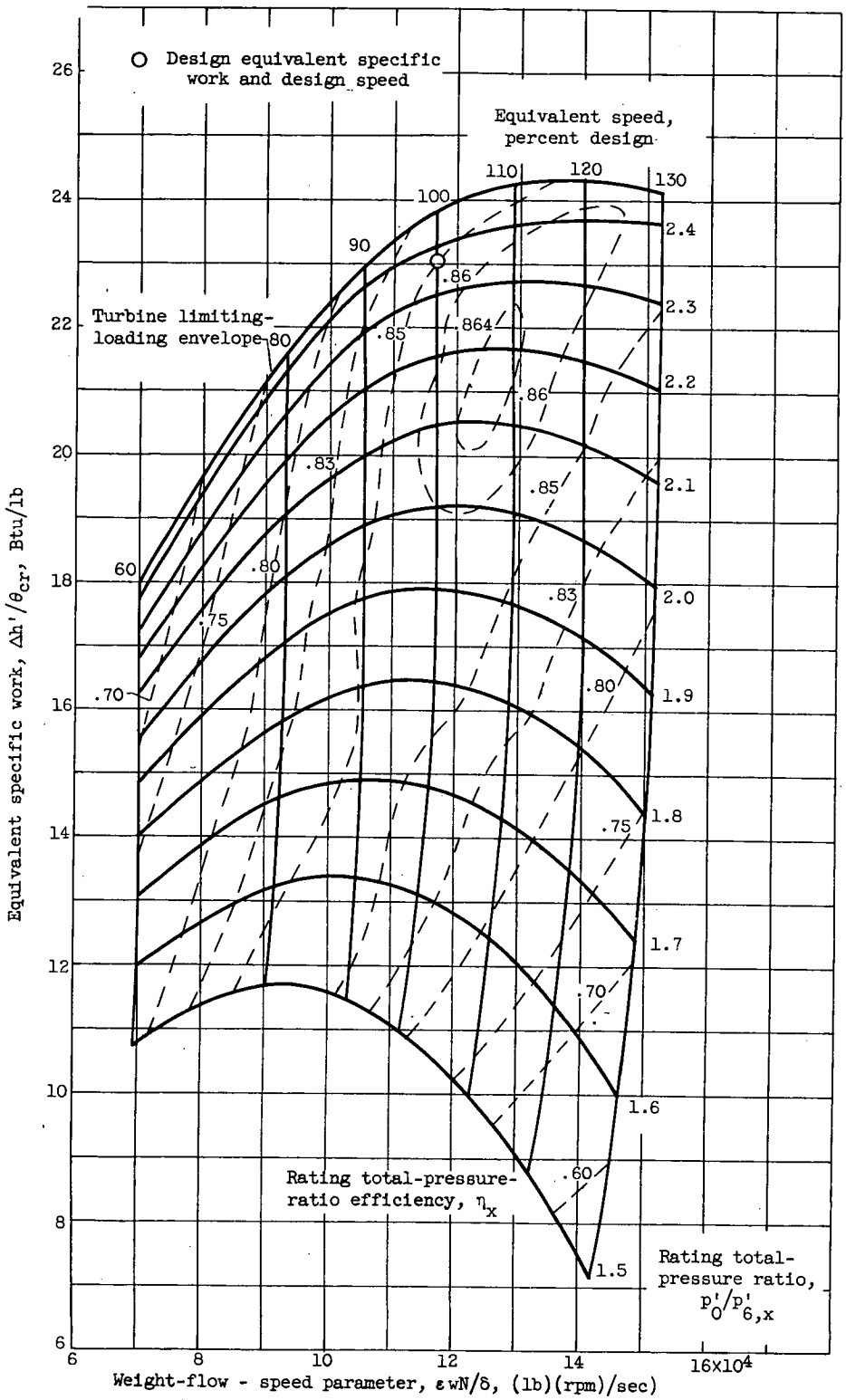

(b) Based on rating total-pressure ratio across turbine.

Figure 7. - Concluded. Experimentally obtained performance map.

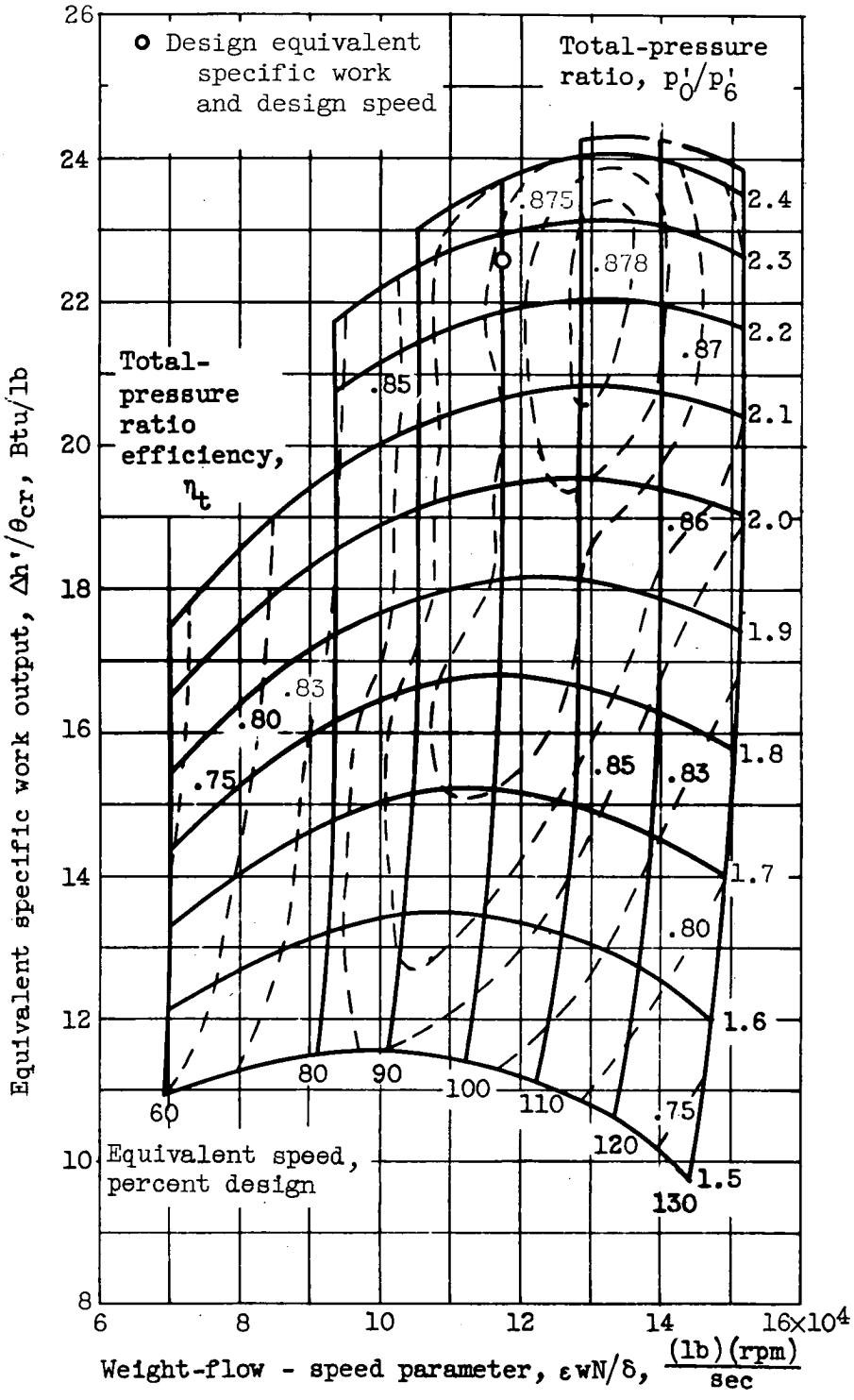

Figure 8. - Performance map based on total-pressure ratio for turbine of reference 6.

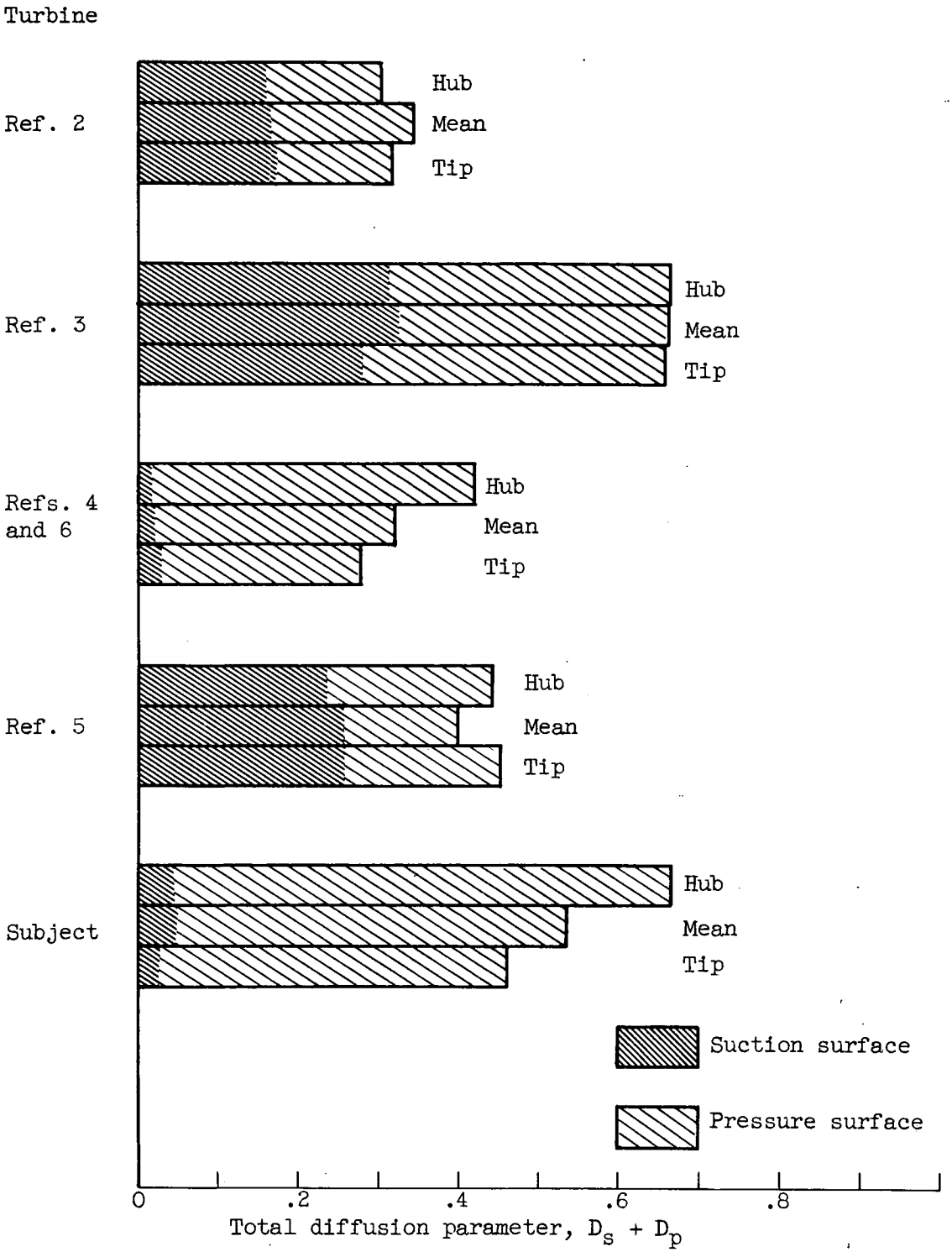

Figure 9. - Sum of suction- and pressure-surface diffusion parameters for five transonic-turbine rotors.

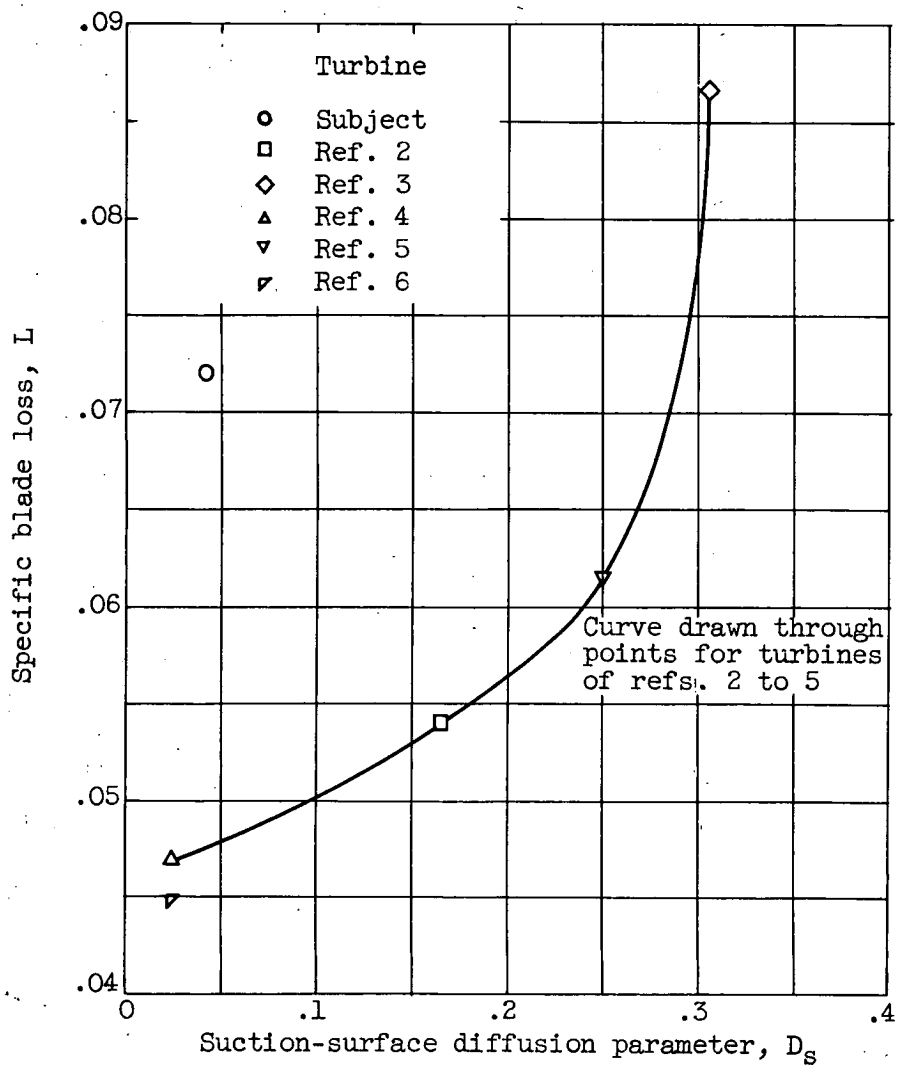

Figure 10. - Effect of suction-surface diffusion parameter on specific blade loss as determined from design-point performance of six transonic-turbine configurations.

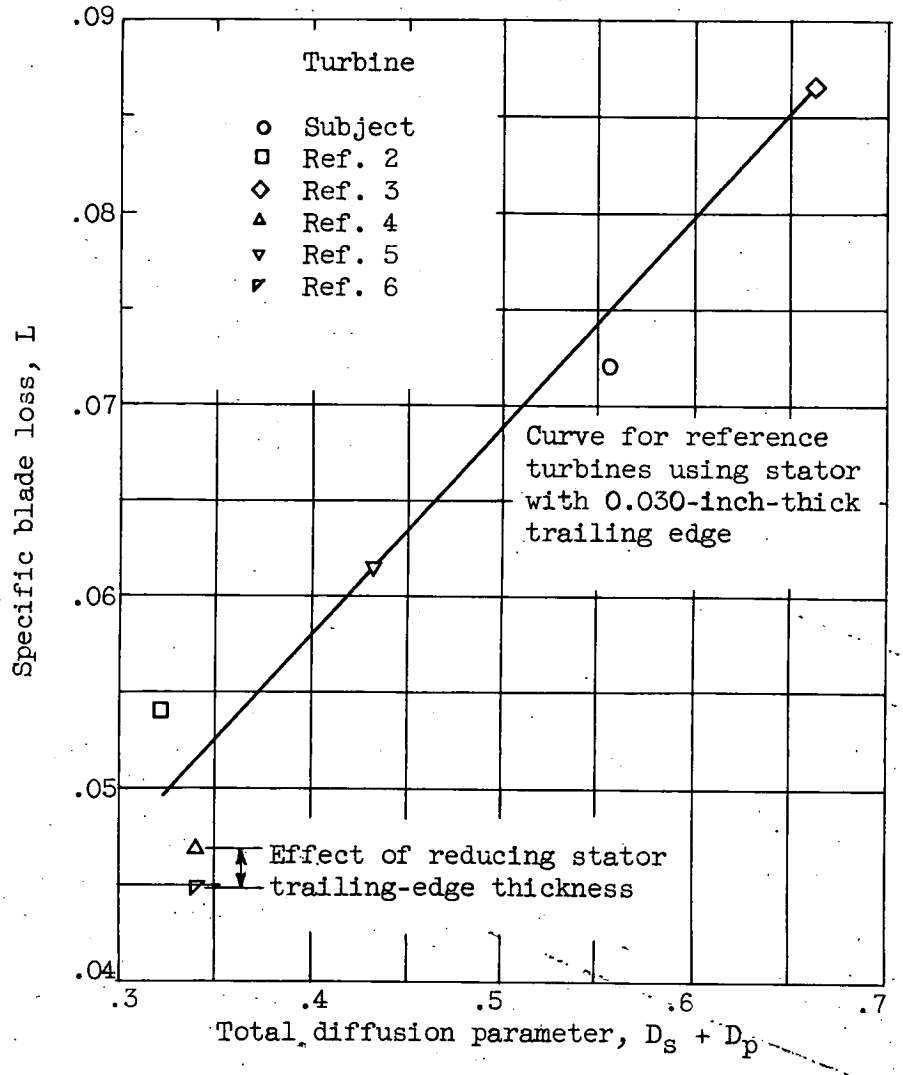

Figure 11. - Effect of total diffusion parameter on specific blade loss as determined from design-point performance of six transonic-turbine configurations.

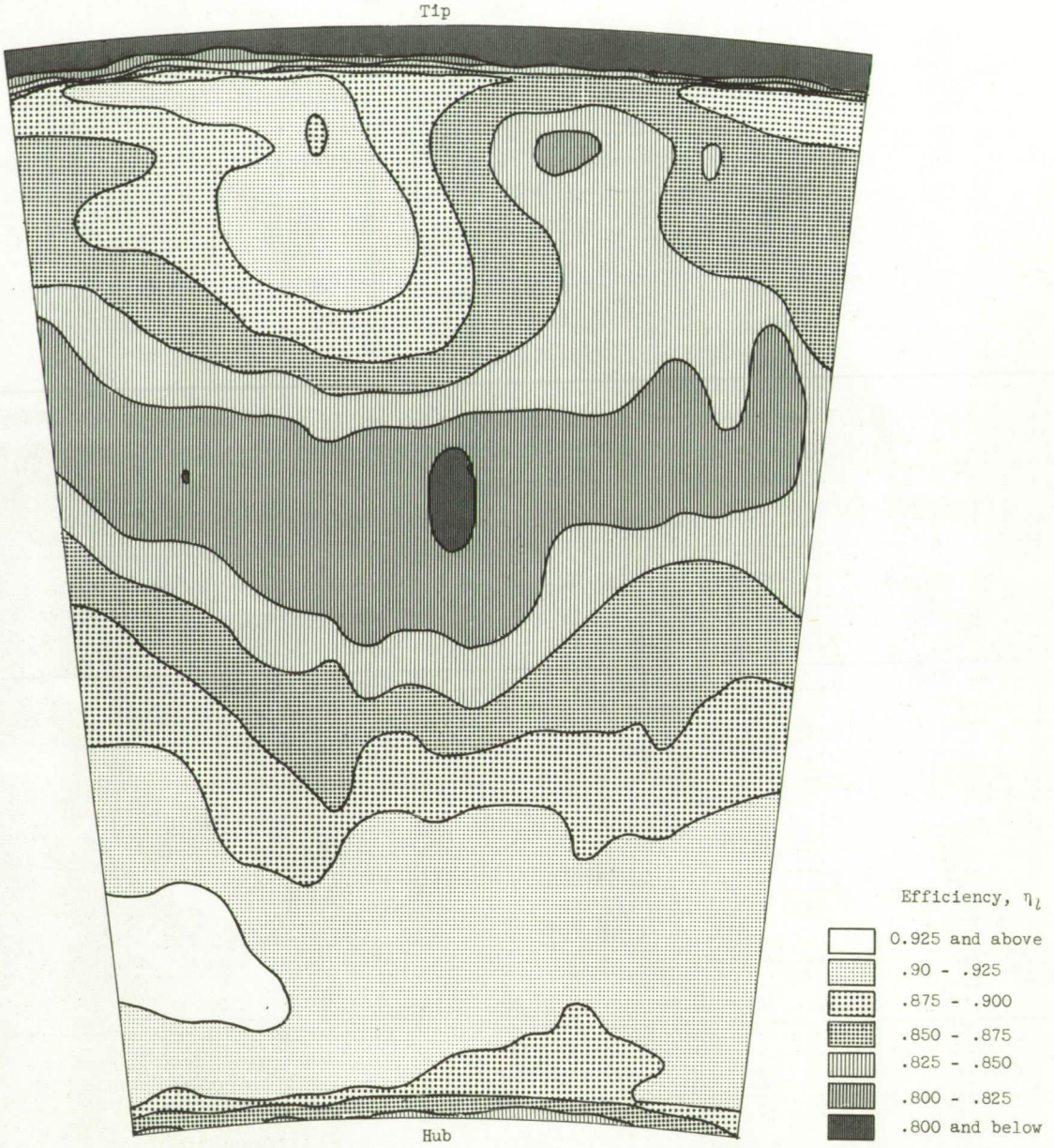

Figure 12. - Contours of local adiabatic efficiency from detailed surveys downstream of rotor at design operating conditions. (Portion of turbine-outlet flow annulus shown corresponds to about $1\frac{1}{4}$ stator passages.)

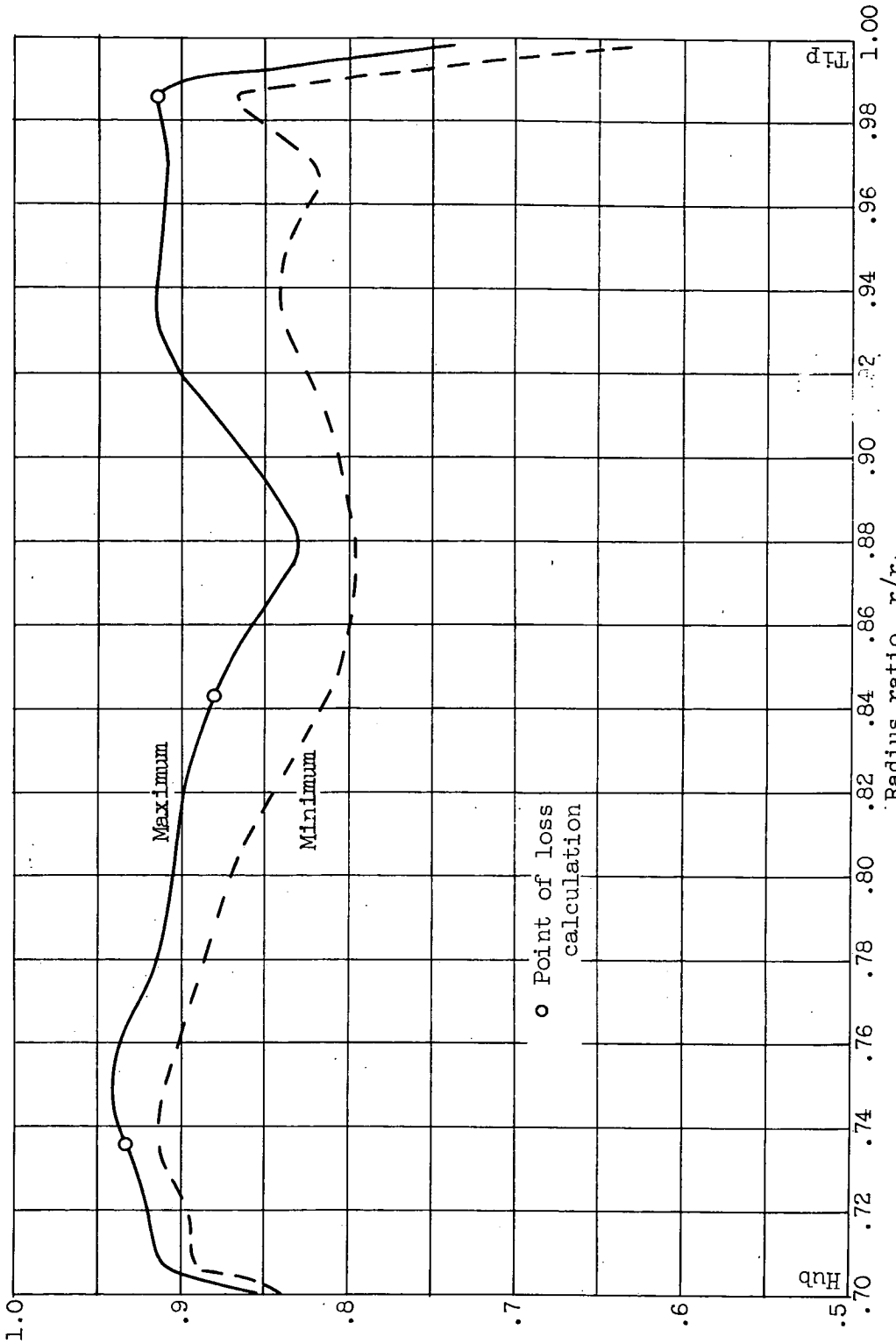

Figure 13. - Variation of maximum and minimum local adiabatic efficiency with radius ratio.

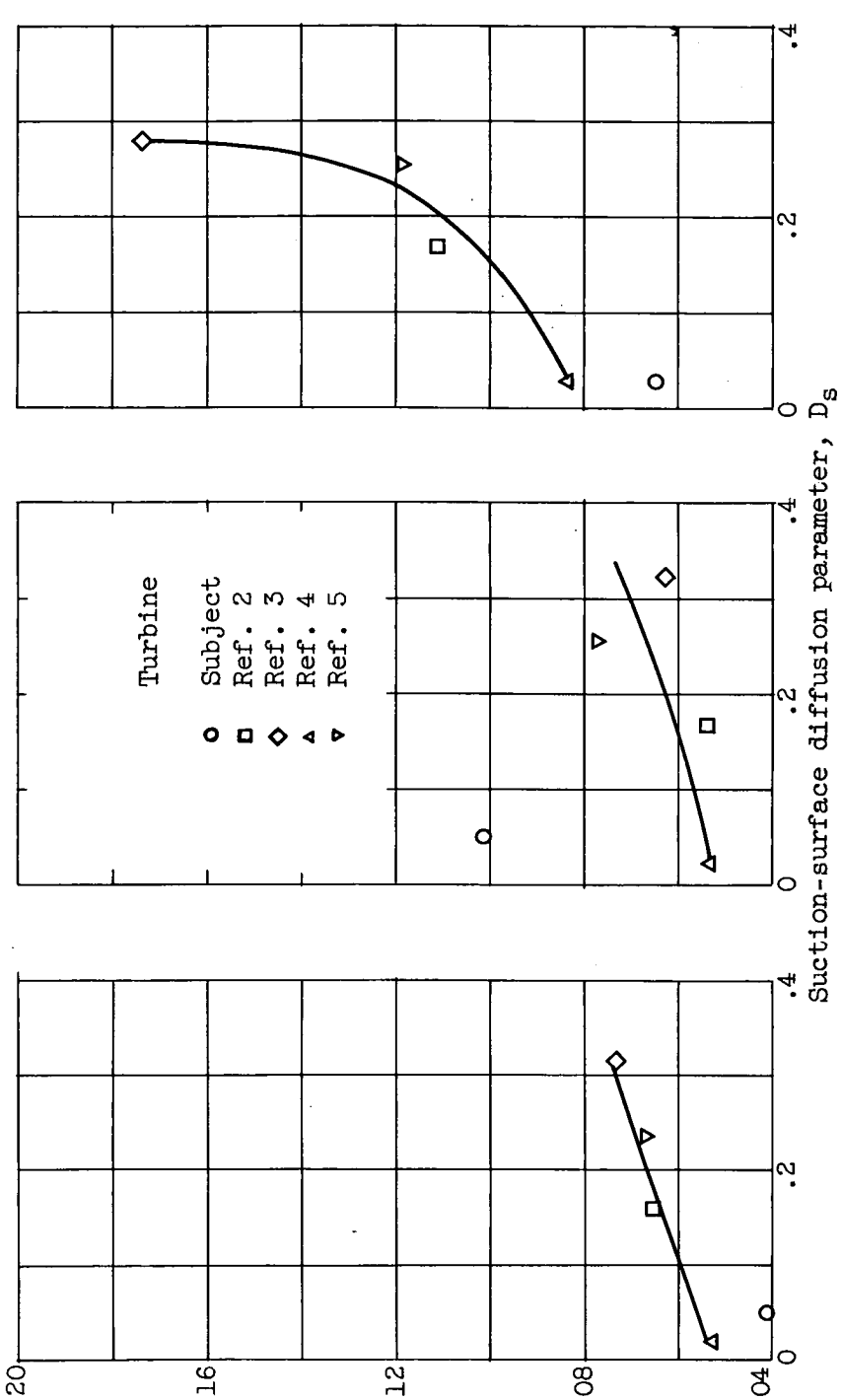

(a) Hub. (b) Mean. (c) Tip.

Figure 14. - Variation of measured blade-element loss parameter with suction-surface diffusion parameter at hub, mean, and tip radii for five transonic turbines. (Curves are those shown in fig. 7 of ref. 9.)

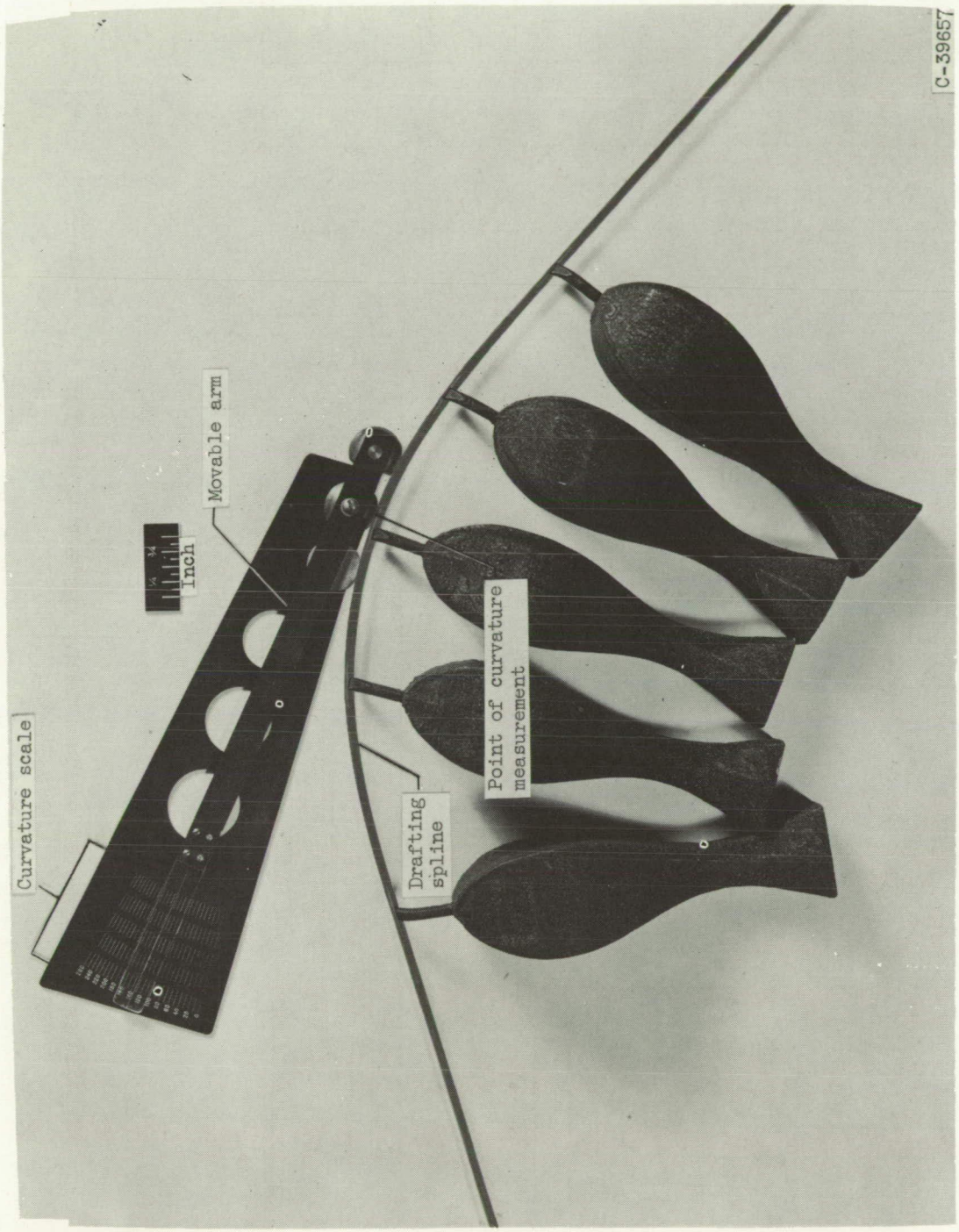

Figure 15. - Photograph of curvometer.